

Supplementary material for

Novel Class of Rhenium Borides Based on Hexagonal Boron Networks Interconnected by Short B₂ Dumbbells

Elena Bykova^{1,2*}, Erik Johansson³, Maxim Bykov^{1,4}, Stella Chariton⁵, Hongzhan Fei², Sergey V. Ovsyannikov², Alena Aslandukova², Stefan Gabel⁶, Hendrik Holz^{6,7}, Benoit Merle^{6,7}, Björn Alling³, Igor A. Abrikosov³, Jesse S. Smith⁸, Vitali B. Prakapenka⁵, Tomoo Katsura², Natalia Dubrovinskaia^{3,9}, Alexander F. Goncharov¹ & Leonid Dubrovinsky²

¹Earth and Planets Laboratory, Carnegie Institution for Science, 5241 Broad Branch Road, NW, Washington DC, 20015, USA

²Bayerisches Geoinstitut, University of Bayreuth, Universitätsstraße 30, 95440, Bayreuth, Germany

³Department of Physics, Chemistry and Biology (IFM), Linköping University, Campus Valla, Fysikhuset, SE-58183, Linköping, Sweden

⁴Institute of Inorganic Chemistry, University of Cologne, Greinstrasse 6, 50939 Cologne, Germany

⁵Center for Advanced Radiation Sources, The University of Chicago, 5640 S. Ellis, Chicago, IL, 60637, USA

⁶Materials Science and Engineering, Institute I, Interdisciplinary Center for Nanostructured Films (IZNF), Friedrich-Alexander-Universität Erlangen-Nürnberg, Cauerstr. 3, D-91058, Erlangen, Germany

⁷Institute of Materials Engineering, University of Kassel, 34125, Kassel, Germany

⁸HPCAT, X-ray Science Division, Argonne National Laboratory, Argonne, Illinois 60439, USA

⁹Material Physics and Technology at Extreme Conditions, Laboratory of Crystallography, University of Bayreuth, Universitätsstraße 30, 95440, Bayreuth, Germany

***Corresponding author e-mail: knilav@gmail.com**

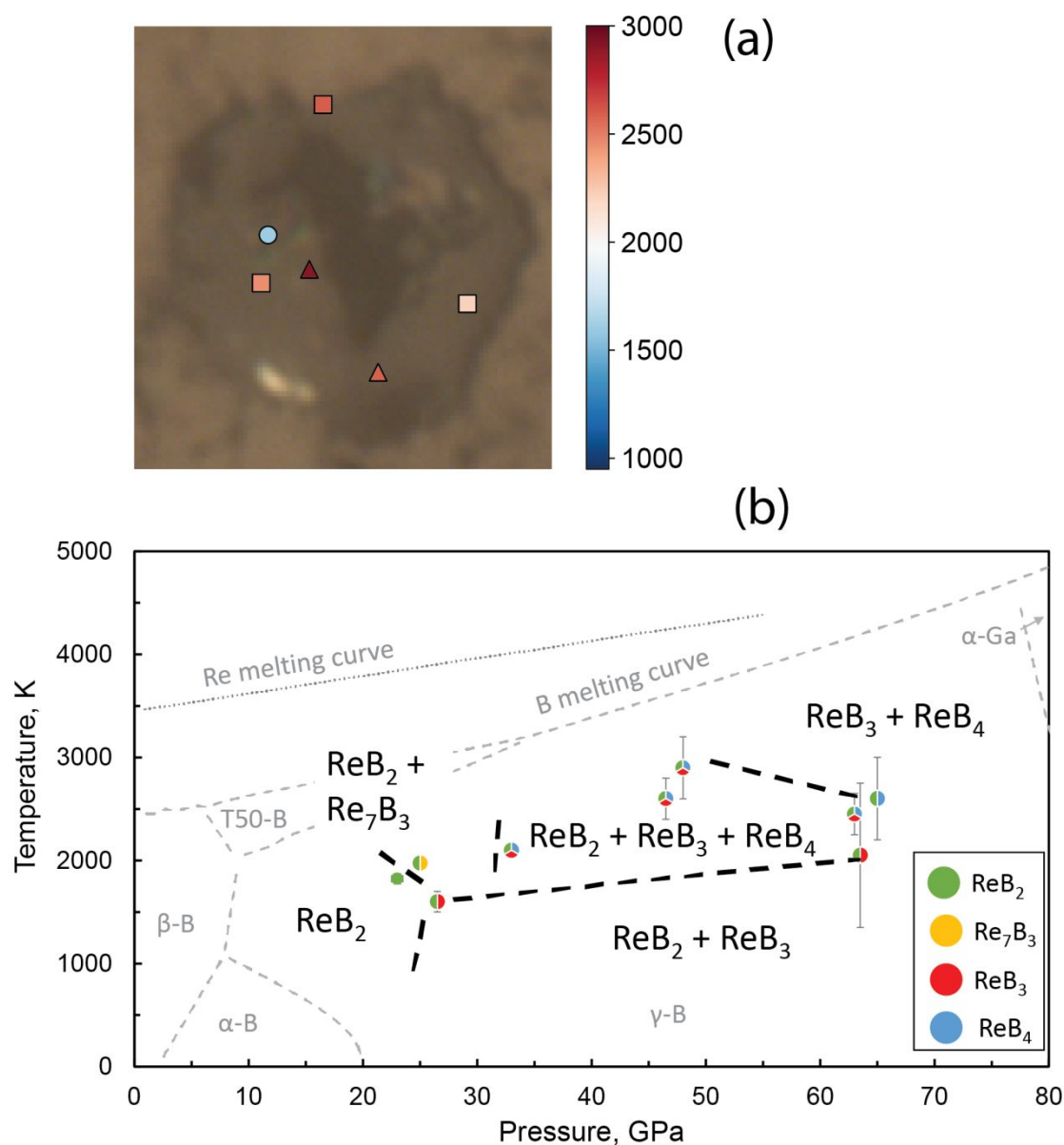


Figure S1. Summary of heating experiments on Re+B mixture. (a) Microphotograph of the sample chamber in a diamond anvil cell showing the positions where laser heating procedures were performed. Marker shape corresponds to a certain pressure range (circles – 26.5; triangles – 46.5-48.0; squares – 63-65 GPa), marker color defines the temperature after which the reaction occurs (temperature values are given in Table S1). (b) Phase compositions of reaction products after the heating at high pressure (circle charts, color represent the particular phase: green – ReB_2 ; yellow – Re_7B_3 ; red – ReB_3 ; blue – ReB_4). Black solid lines are only guides for an eye and may not represent actual phase boundaries. Grey dash lines show phase boundaries in pure boron¹ and a melting curve of pure rhenium².

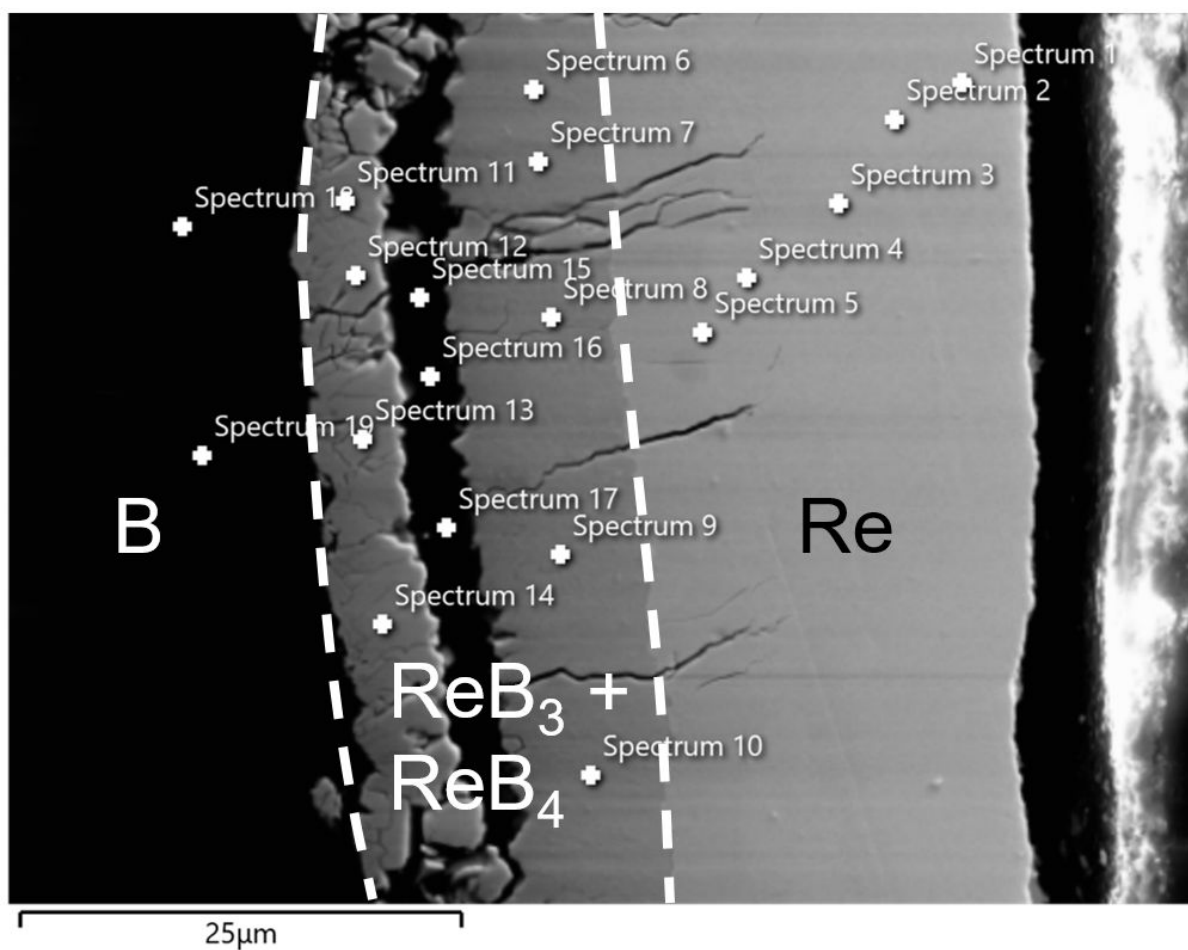


Figure S2. The SEM image of the sample obtained in the HPHT synthesis in multi-anvil apparatus 33 GPa and 2073-2123 K. White crosses show the positions on sample at which the data on chemical composition was collected. The central part of the image (dark grey field) shows mixture of ReB₃ and ReB₄ produced due to a reaction between Re with B. Black left part of image correspond to non-reacted boron which, however, underwent a pressure-induced phase transformation from β -B to γ -B. Right light-grey field is non-reacted rhenium.

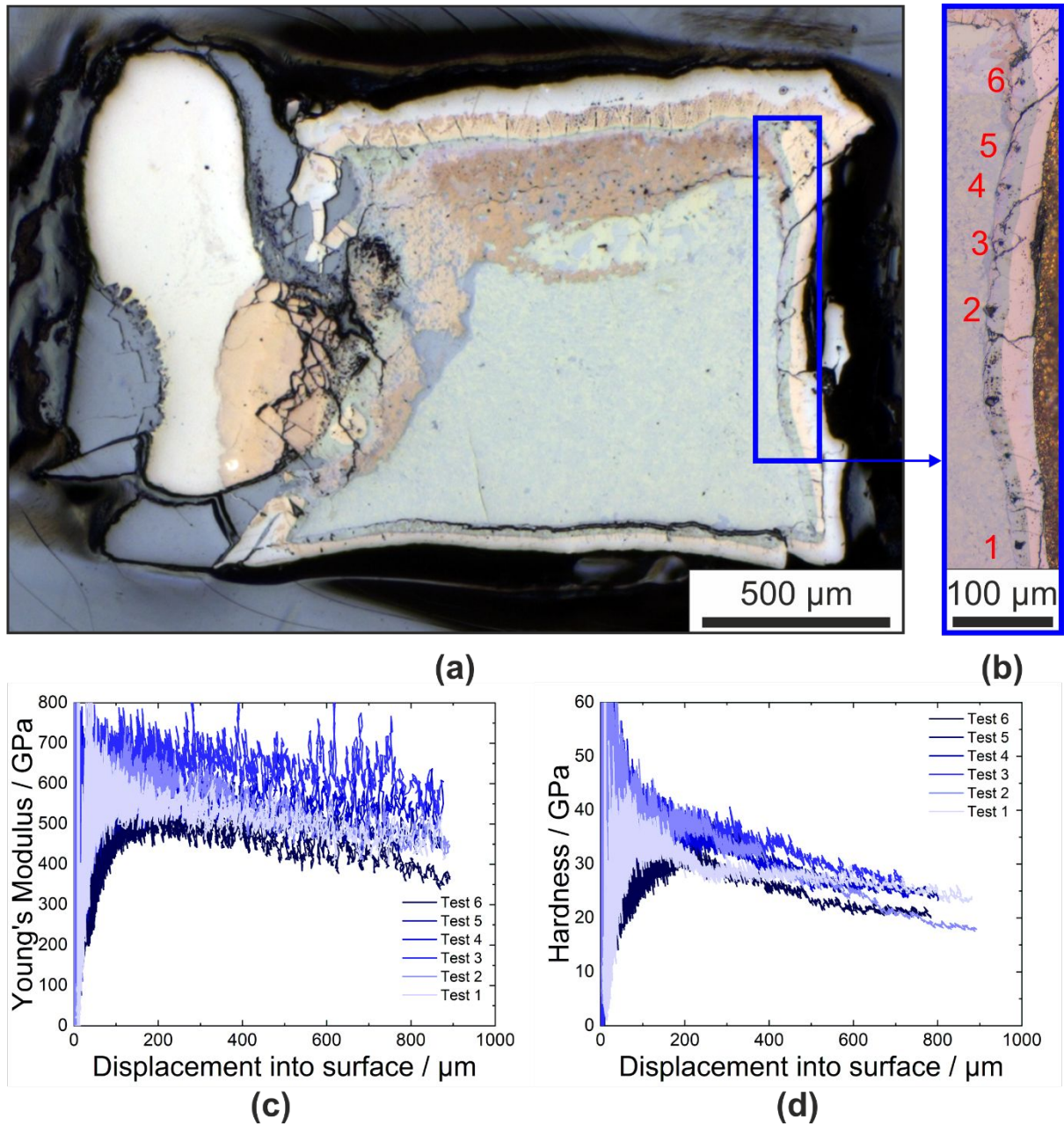


Figure S3. Summary of the nanoindentation measurements. Microphotograph of the polished part of the capsule retrieved after synthesis at 33 GPa (a) with blue rectangle showing the area at which nanoindentation measurements were performed. Enlarged image of the area (b) and numbers corresponding to the indentation sites. Variation of Young's modulus (c) and hardness with indentation depth (d), the decrease at large indentation depth is due to ongoing fracturation of the material around the indents.

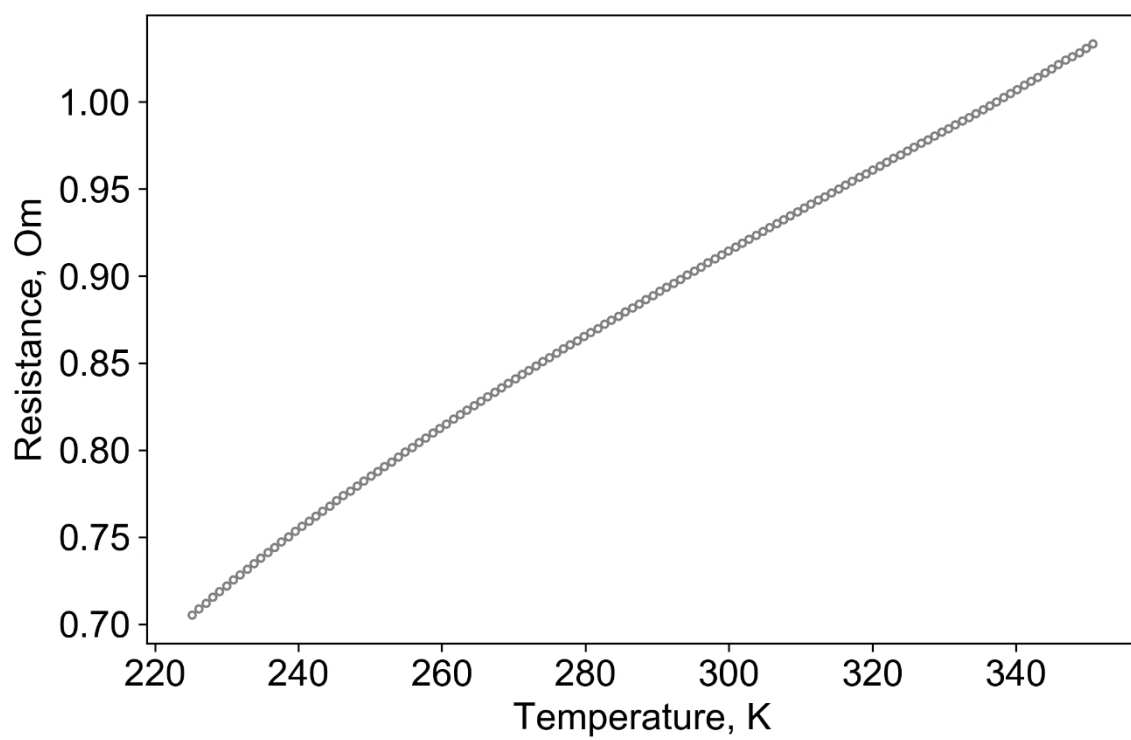


Figure S4. Electrical resistance of a particle containing ReB_3 and ReB_4 showing a metallic behaviour.

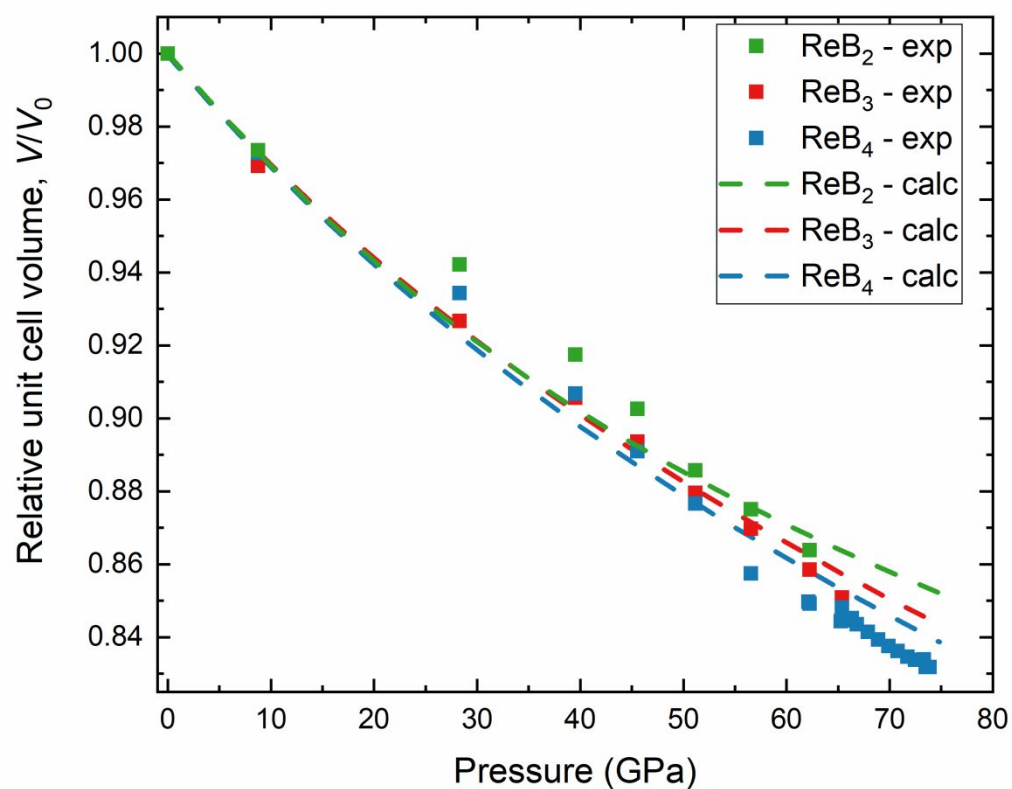


Figure S5. Comparison between relative volume compressibilities of ReB_2 (green), ReB_3 (red) and ReB_4 (blue). Solid filled symbols represent experimental data, dash lines correspond to the values computed by DFT.

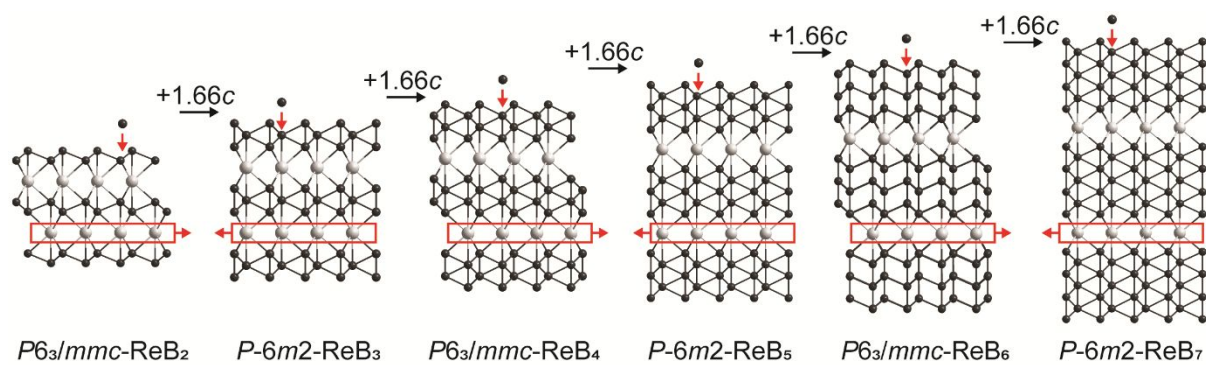


Figure S6. Generation of homologous ReB_x ($x > 2$) compounds by adding boron atoms with the short bonds oriented parallel to c -axis to boron chair-like hexagonal sheets.

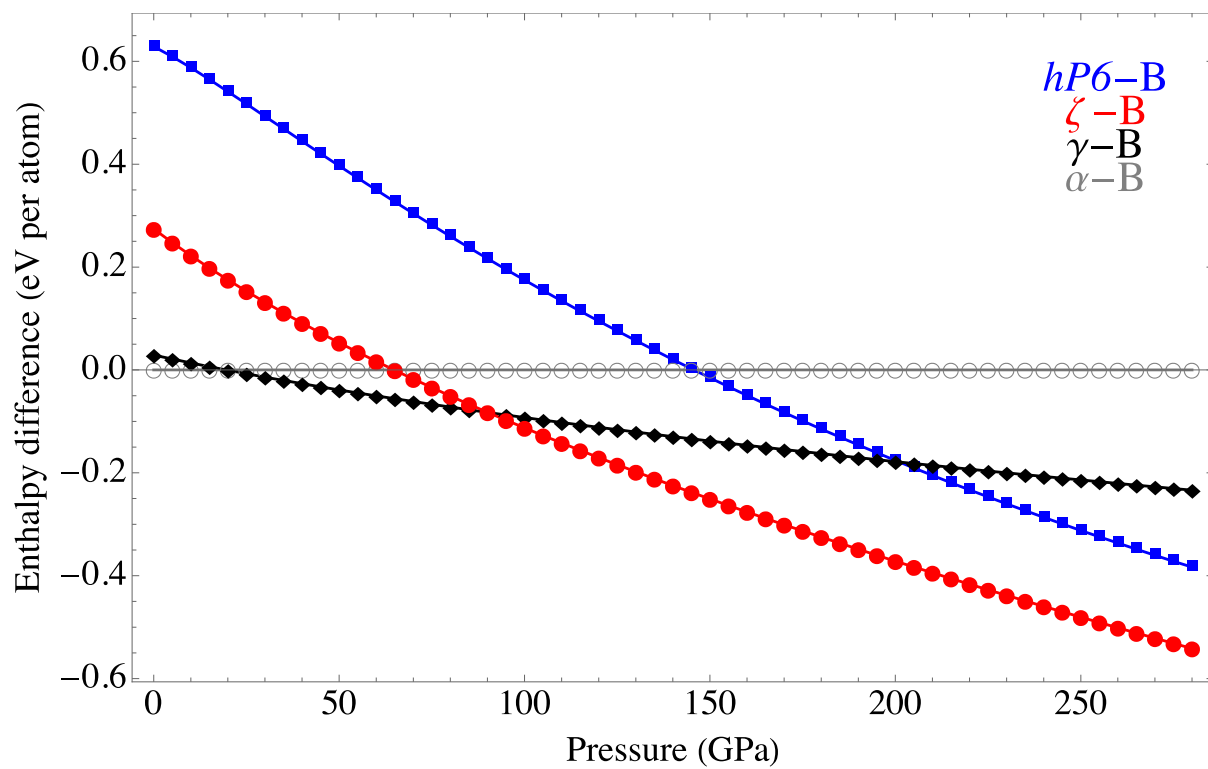
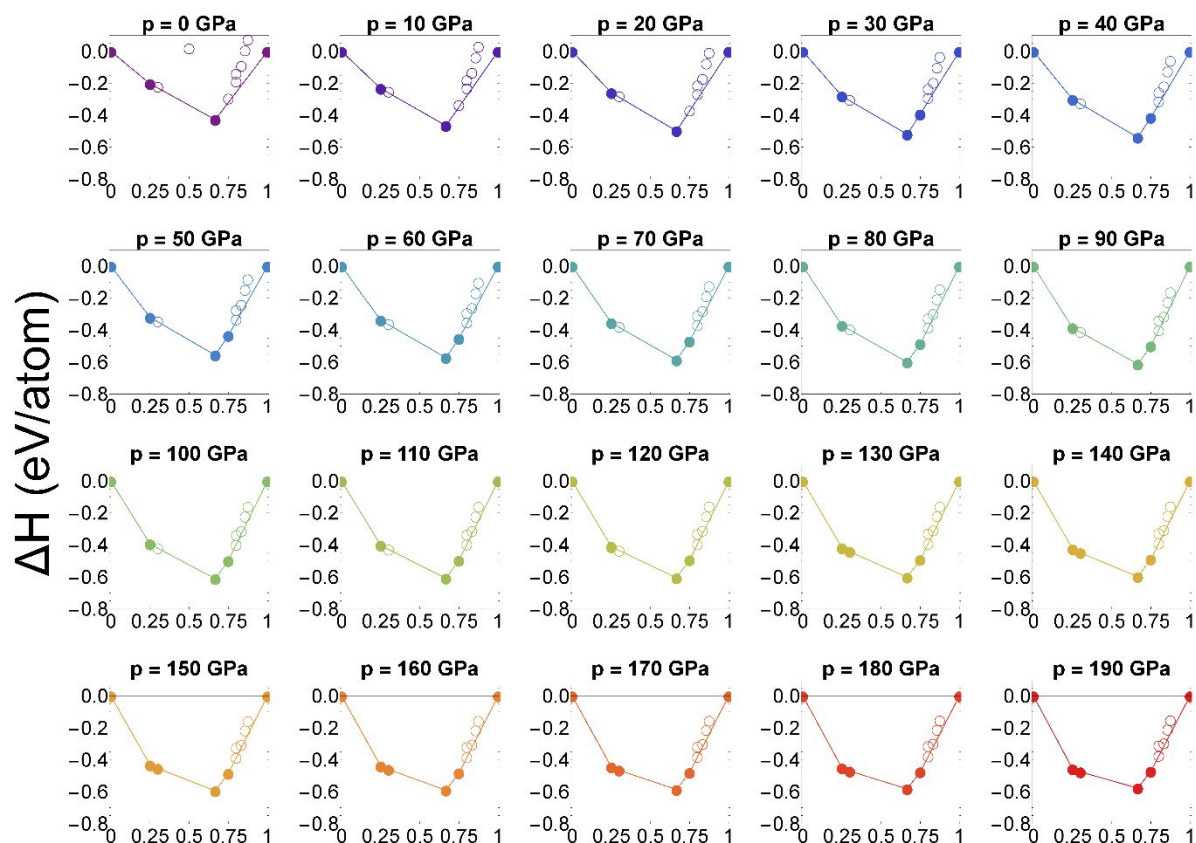


Figure S7. Calculated enthalpy curves of γ -, ζ -(α -Ga type) and $hP6$ -boron relative to α -B as a function of pressure.



B composition

Figure S8. Thermodynamic convex hull of Re–B system from 0 GPa up to 190 GPa in steps of 10 GPa, at 0 K. Filled circles are stable phases sitting on the convex hull, open circles are metastable ones. Following crystal structures were considered: Re; Re_3B ; Re_7B_3 ; ReB_2 ; ReB_3 ($P6_3/mmc$); ReB_4 ($P6_3/mmc$ and $R-3m$); ReB_5 ; ReB_6 ; ReB_7 ; B (α -B – below 19 GPa; γ -B – between 19 and 90 GPa; ζ -(α -Ga type) – above 90 GPa). $R-3m$ - ReB_4 proposed in Ref.³ was always found much higher in enthalpy compared to $P6_3/mmc$.

Table S1. Experimental conditions in laser heating experiments in DAC and in multi-anvil apparatus.

Initial phase composition	Pressure range, GPa	Temperature range, K	Final phase composition	
Laser-heating experiments in DAC				
β -B, γ -B, Re	26.5(5)	1600(100)	γ -B, ReB ₂ , ReB ₃	
γ -B, Re	46.5(5)	2600(200)	γ -B, ReB ₂ , ReB ₃ , ReB ₄	
γ -B, Re	48.0(5)	2900(300)	γ -B, ReB ₂ , ReB ₃ , ReB ₄	
γ -B, Re	63.5(5)	2050(700)	γ -B, ReB ₂ , ReB ₃	
γ -B, ReB ₂ , ReB ₃	63.0(5)	2450(200)	γ -B, ReB ₂ , ReB ₃ , ReB ₄	
γ -B, Re	65.0(5)	2600(400)	γ -B, ReB ₂ , ReB ₄	
Multi-anvil experiments				
Initial phase composition	Pressure range, GPa	Temperature range, K	Heating duration, hours	Final phase composition
Amorphous boron + Re	20	1773-1873	24	ReB ₂
Amorphous boron + Re	23	1973	24	ReB ₂ , Re ₇ B ₃
Amorphous boron + Re	33	2073-2123	5	γ -B, ReB ₂ , ReB ₃ , ReB ₄

Table S2. Details of crystal structure refinements for ReB₃ at high pressures (sp.gr. *P-6m2*; *Z* = 1; Re1 *1a* (0, 0, 0), B1 *1b* (0, 0, 0.5), B2 *2h* (1/3, 2/3, *z*))

Pressure, GPa	62.3(5)	56.6(5)	45.5(5)	39.5(5)	28.3(5)	8.8(5)	0.0001
<i>a</i> (Å)	2.7544(6)	2.7607(8)	2.7933(8)	2.8004(5)	2.8220(6)	2.8855(12)	2.9075(3)
<i>c</i> (Å)	4.4322(10)	4.4653(15)	4.4541(9)	4.4686(6)	4.5104(6)	4.5573(11)	4.5783(4)
<i>V</i> (Å ³)	29.120(14)	29.473(19)	30.096(17)	30.349(12)	31.107(14)	32.86(3)	33.519(8)
ρ_{calc} (g/cm ³)	12.467	12.318	12.063	11.962	11.671	11.048	10.831
μ/mm^{-1}	15.47	15.285	14.969	14.844	14.482	13.71	13.578
$2\Theta_{\text{min}}$ for data collection (°)	4.141	4.132	2.216	2.209	2.189	2.166	2.156
$2\Theta_{\text{max}}$ for data collection (°)	15.815	16.523	15.664	15.75	16.74	15.392	15.74
Completeness to <i>d</i> = 0.8 Å	0.792	0.72	0.8	0.8	0.846	0.815	0.926
Reflections collected	64	62	62	69	69	68	65
Independent reflections	43	40	37	38	43	40	46
Independent reflections [<i>I</i> > 2σ(<i>I</i>)]	43	40	37	38	43	40	46
Refined parameters	6	6	6	6	6	6	6
<i>R</i> _{int} (<i>F</i> ²)	0.0159	0.0217	0.0244	0.0149	0.0185	0.0374	0.0681
<i>R</i> (σ)	0.0269	0.0214	0.0214	0.017	0.0215	0.0385	0.0403
<i>R</i> ₁ [<i>I</i> > 2σ(<i>I</i>)]	0.0341	0.0267	0.04	0.0208	0.0334	0.043	0.0462
<i>wR</i> ₂ [<i>I</i> > 2σ(<i>I</i>)]	0.0718	0.0636	0.0928	0.0448	0.0746	0.1015	0.1267
<i>R</i> ₁	0.0341	0.0267	0.04	0.0208	0.0334	0.043	0.0462
<i>wR</i> ₂	0.0718	0.0636	0.0928	0.0448	0.0746	0.1015	0.1267
Goodness of fit on <i>F</i> ²	1.171	1.355	1.37	1.218	1.15	1.379	1.276
$\Delta\rho_{\text{max}}$ (<i>e</i> / Å ³)	2.833	1.935	3.541	1.887	2.945	2.669	2.983
$\Delta\rho_{\text{min}}$ (<i>e</i> / Å ³)	-2.42	-2.942	-5.857	-2.099	-2.895	-5.012	-4.301
<i>z</i> (B2)	0.320(13)	0.313(11)	0.311(17)	0.310(7)	0.311(12)	0.321(16)	-0.32(2)
<i>U</i> _{eq} (Re1) (Å ²)*	0.0041(7)	0.0055(5)	0.0068(8)	0.0044(4)	0.0044(5)	0.0124(10)	0.0049(9)
<i>U</i> _{iso} (B1) (Å ²)	0.003(9)	0.008(8)	0.010(12)	0.005(6)	0.012(11)	0.011(16)	0.008(15)
<i>U</i> _{iso} (B2) (Å ²)	0.006(12)	0.002(6)	0.015(13)	0.006(7)	0.013(11)	0.015(18)	0.014(16)
<i>dI</i> (Re1...B2) (Å)	2.13(4)	2.12(3)	2.13(5)	2.13(2)	2.15(4)	2.22(5)	2.23(6)
<i>d2</i> (Re1...B1) (Å)	2.2161(5)	2.2327(8)	2.2271(4)	2.2343(3)	2.2552(3)	2.2787(5)	2.2892(2)
<i>d3</i> (B2–B2) (Å)	1.60(12)	1.67(10)	1.68(15)	1.70(6)	1.70(11)	1.63(15)	1.64(18)
<i>d4</i> (B1–B2) (Å)	1.78(3)	1.80(2)	1.82(4)	1.826(15)	1.84(3)	1.86(3)	1.87(4)
Data collection	APS, 16-IDB beamline, Pilatus Si 1M-F detector, λ = 0.34453 Å						
ICSD number	2151329	2151328	2151327	2151326	2151325	2151324	2151323

**U*_{eq} is defined as one third of the trace of the orthogonalized *U*^{ij} tensor.

Table S3. Structural data for ReB₄ at high pressures (sp.gr. *P6₃/mmc*; *Z* = 2; Re1 2*d* (2/3, 1/3, 1/4), B1 4*f*(1/3, 2/3, *z*), B2 4*f*(1/3, 2/3, *z*))

Pressure, GPa	75.0(5)	63.7(5)	58.4(5)	51.8(5)	47.5(5)	44.3(5)	39.5(5)	33.1(5)	28.3(5)	9.4(5)	8.8(5)	0.0001
<i>a</i> (Å)	2.7349(14)	2.7615(12)	2.778(2)	2.7928(17)	2.8132(19)	2.807(3)	2.813(7)	2.829(4)	2.8387(18)	2.861(2)	2.9206(18)	2.9333(18)
<i>c</i> (Å)	10.368(11)	10.480(9)	10.507(5)	10.516(4)	10.510(6)	10.68(2)	10.592(16)	10.73(3)	10.572(3)	10.684(5)	10.53(7)	10.838(3)
<i>V</i> (Å ³)	67.16(10)	69.21(8)	70.22(12)	71.03(9)	72.04(11)	72.9(2)	72.6(4)	74.4(3)	73.78(10)	75.75(13)	77.8(5)	80.76(10)
ρ_{calc} (g/cm ³)	11.346	11.009	10.851	10.727	10.578	10.453	10.495	10.249	10.328	10.06	9.793	9.435
μ/mm^{-1}	8.957	13.028	12.841	12.693	12.517	12.37	12.419	12.127	12.222	11.904	11.589	11.165
2 Θ_{min} for data collection (°)	3.573	4.131	1.879	1.877	1.879	4.063	1.864	4.032	3.737	3.698	3.905	1.822
2 Θ_{max} for data collection (°)	14.531	16.997	16.535	16.5	16.477	16.099	16.752	17.296	15.529	17.041	15.72	16.751
Completeness to <i>d</i> = 0.8 Å	0.732	0.721	0.773	0.778	0.711	0.674	0.674	0.702	0.638	0.729	0.51	0.857
Reflections collected	132	108	121	129	115	118	112	122	116	113	148	155
Independent reflections	58	55	53	55	54	47	44	50	46	57	39	72
Independent reflections [<i>I</i> > 2 σ (<i>I</i>)]	55	51	53	55	54	42	43	45	44	57	35	68
Refined parameters	7	7	7	7	7	7	7	7	7	7	7	7
<i>R</i> _{int} (<i>F</i> ²)	0.0135	0.0091	0.0138	0.0119	0.0148	0.0237	0.0407	0.0229	0.0403	0.0145	0.0466	0.0165
<i>R</i> (σ)	0.013	0.0092	0.0143	0.0167	0.017	0.017	0.0354	0.0192	0.0363	0.0167	0.0302	0.0144
<i>R</i> ₁ [<i>I</i> > 2 σ (<i>I</i>)]	0.0257	0.0244	0.0304	0.0275	0.0266	0.0289	0.0377	0.0267	0.0389	0.0361	0.0215	0.0262
<i>wR</i> ₂ [<i>I</i> > 2 σ (<i>I</i>)]	0.068	0.061	0.0731	0.0712	0.0643	0.0669	0.0916	0.0647	0.0964	0.0896	0.0486	0.0703
<i>R</i> ₁	0.0257	0.0263	0.0304	0.0275	0.0266	0.0299	0.0417	0.0311	0.0411	0.0361	0.0298	0.0285
<i>wR</i> ₂	0.0682	0.0633	0.0731	0.0712	0.0643	0.0686	0.0932	0.0653	0.0967	0.0896	0.0492	0.0717
Goodness of fit on <i>F</i> ²	1.27	1.25	1.226	1.307	1.174	1.206	1.231	1.25	1.212	1.119	1.126	1.313
$\Delta\rho_{\text{max}}$ (<i>e</i> / Å ³)	3.528	2.255	4.901	4.742	4.152	2.804	2.427	1.874	4.121	4.271	1.218	2.561
$\Delta\rho_{\text{min}}$ (<i>e</i> / Å ³)	-3.595	-2.292	-4.124	-2.294	-2.309	-2.083	-2.384	-1.671	-3.588	-2.562	-1.172	-2.348
<i>z</i> (B1)	0.539(3)	0.541(2)	0.541(2)	0.542(2)	0.543(2)	0.543(4)	0.536(3)	0.543(4)	0.540(4)	0.542(3)	0.540(4)	0.542(2)
<i>z</i> (B2)	0.116(3)	0.114(2)	0.111(3)	0.114(3)	0.112(3)	0.117(3)	0.121(3)	0.115(3)	0.112(5)	0.118(3)	0.119(5)	0.1166(19)
<i>U</i> _{eq} (Re1) (Å ²)*	0.0036(3)	0.0014(3)	0.0060(4)	0.0036(4)	0.0053(4)	0.0047(4)	0.0076(7)	0.0061(4)	0.0066(8)	0.0132(5)	0.0064(6)	0.0039(3)
<i>U</i> _{iso} (B1) (Å ²)	0.005(4)	0.001(3)	0.009(4)	0.004(4)	0.006(3)	0.008(5)	0.002(6)	0.012(5)	0.012(8)	0.015(5)	0.003(3)	0.009(4)
<i>U</i> _{iso} (B2) (Å ²)	0.008(4)	0.005(4)	0.013(5)	0.011(5)	0.015(5)	0.005(4)	0.006(6)	0.007(4)	0.027(12)	0.013(5)	0.007(4)	0.006(3)
<i>d</i> 1(Re1...B2) (Å)	2.11(2)	2.140(17)	2.171(19)	2.158(18)	2.178(18)	2.15(2)	2.12(2)	2.18(2)	2.20(4)	2.17(2)	2.18(3)	2.226(14)
<i>d</i> 2(Re1...B1) (Å)	2.18(3)	2.20(2)	2.19(3)	2.18(2)	2.18(2)	2.21(4)	2.27(3)	2.22(4)	2.22(4)	2.22(3)	2.21(4)	2.25(2)
<i>d</i> 3(B1–B2) #1 (Å)	1.61(4)	1.62(3)	1.60(4)	1.64(4)	1.63(4)	1.71(5)	1.66(5)	1.69(5)	1.61(7)	1.71(5)	1.67(7)	1.72(3)
<i>d</i> 4(B1–B2) #2 (Å)	1.77(2)	1.770(15)	1.761(14)	1.778(13)	1.779(13)	1.80(2)	1.79(2)	1.81(2)	1.80(3)	1.841(19)	1.88(3)	1.877(14)
<i>d</i> 5(B1–B1) (Å)	1.78(3)	1.81(2)	1.82(2)	1.84(2)	1.86(2)	1.86(4)	1.86(2)	1.87(4)	1.85(4)	1.88(3)	1.89(4)	1.92(2)
Data collection	(1)	(2)	(2)	(2)	(2)	(2)	(2)	(2)	(2)	(2)	(2)	(2)
ICSD number	2151341	2151340	2151339	2151338	2151337	2151336	2151335	2151334	2151333	2151332	2151331	2151330

**U*_{eq} is defined as one third of the trace of the orthogonalized *U*^{ij} tensor.

(1) APS, 13-ID-D beamline, Pilatus CdTe 1M detector, λ = 0.29521 Å

(2) APS, 16-ID-B beamline, Pilatus Si 1M-F detector, λ = 0.34453 Å

Table S4. Optimized crystal structures of ReB_x ($x = 5-7$) and $hP6$ -boron at ambient pressure

Phase	Lattice parameters		Coordinates			
	a , Å	c , Å	Atom	x	y	z
$P\text{-}6m2\text{-}\text{ReB}_5$	2.93673	6.28848	Re1	0	0	0
			B1	0	0	0.359
			B2	0	0	0.630
			B3	1/3	2/3	0.231
			B4	1/3	2/3	0.769
			B5	1/3	2/3	0.500
$P6_3/mmc\text{-}\text{ReB}_6$	2.93312	14.3243	Re1	2/3	1/3	0.250
			Re2	1/3	2/3	0.750
			B1	1/3	2/3	0.592
			B2	2/3	1/3	0.408
			B3	2/3	1/3	0.092
			B4	1/3	2/3	0.908
			B5	1/3	2/3	0.148
			B6	2/3	1/3	0.852
			B7	2/3	1/3	0.648
			B8	1/3	2/3	0.352
			B9	1/3	2/3	0.470
			B10	2/3	1/3	0.530
			B11	2/3	1/3	0.970
			B12	1/3	2/3	0.030
$P\text{-}6m2\text{-}\text{ReB}_7$	2.93316	8.02968	Re1	0	0	0
			B1	0	0	0.5
			B2	1/3	2/3	0.392
			B3	1/3	2/3	0.608
			B4	0	0	0.282
			B5	0	0	0.718
			B6	1/3	2/3	0.182
			B7	1/3	2/3	0.818
$P6_3/mmc\text{-B}$	2.87742	5.34790	B1	1/3	2/3	0.250
			B2	2/3	1/3	0.750
			B3	2/3	1/3	0.083
			B4	1/3	2/3	0.917
			B5	1/3	2/3	0.583
			B6	2/3	1/3	0.417

REFERENCES

- (1) Zhang, S.; Whitley, H. D.; Ogitsu, T. Phase Transformation in Boron under Shock Compression. *Solid State Sci.* **2020**, *108*, 106376. <https://doi.org/10.1016/j.solidstatesciences.2020.106376>.
- (2) Yang, L.; Karandikar, A.; Boehler, R. Flash Heating in the Diamond Cell: Melting Curve of Rhenium. *Rev. Sci. Instrum.* **2012**, *83* (6), 2–7. <https://doi.org/10.1063/1.4730595>.
- (3) Wang, B.; Wang, D. Y.; Wang, Y. X. A New Hard Phase of ReB₄ Predicted from First Principles. *J. Alloys Compd.* **2013**, *573*, 20–26. <https://doi.org/10.1016/j.jallcom.2013.03.181>.